Modeling and Simulation of the Operation of an ^{18}O Isotope Separation Cascade using Artificial Intelligence

Laurentiu Chifor*, Vlad Muresan*, Mihaela-Ligia Unguresan, Mihail Abrudean*, Honoriu Vălean*, Iulia Clitan*, Valentin Sita***

** Automation Department, Technical University of Cluj-Napoca, 28 Memorandumului Street, 400114 Cluj-Napoca, Romania (e-mail: Laurentiu.Chifor@aut.utcluj.ro, Vlad.Muresan@aut.utcluj.ro, Mihai.Abrudean@aut.utcluj.ro, Honoriu.Valean@aut.utcluj.ro, Iulia.Clitan@aut.utcluj.ro, Valentin.Sita@aut.utcluj.ro)*

*** Physics and Chemistry Department, Technical University of Cluj-Napoca, 28 Memorandumului Street, 400114 Cluj-Napoca, Romania (e-mail: mihaela.unguresan@chem.utcluj.ro)*

Corresponding Author: mihaela.unguresan@chem.utcluj.ro

Abstract: The manuscript introduces an innovative method for modeling and simulation of the ^{18}O isotope concentrations dynamics inside a separation cascade which contains within its structure 2 separation columns. The proposed model is designed as a nonlinear distributed parameter one. The present study, in order to maximize the model accuracy, does not use simplification and linearization techniques. The functional form of the separation cascade structure parameters is established through unique identification procedures, which rely on experimental data obtained from the real plant. A major difficulty in the study approach was the experimental data take-off, taking into account that the considered separation process is a very slow one and it has strict operation conditions. Due to the nonlinearity of the functions which describe the structure parameters of the plant, two neural networks are used to establish their dynamics. The two neural networks are included in the proposed model to facilitate simulation capabilities. The validation of the model is made through simulation as well as the comparison of the obtained results with the experimental data. Also, the suggested model is simulated in various feasible alternatives, thus resulting in some interesting interpretations and conclusions.

Keywords: Separation Cascade, Modeling, Simulation, Neural Network, ^{18}O, Separation Column.

1. INTRODUCTION

Isotopes, having the same protons and electrons but varying neutron numbers, occupy identical positions in the periodic system, yet possess different mass numbers. Isotope nuclei may be stable or unstable (radioactive), finding diverse applications in agriculture, medicine, and chemistry. The isotopes are used in agriculture, medicine, chemistry, etc. (Abrudean et al., 1981; Cohen, 1951; Dulf et al., 2006; Abrudean et al., 1978) requires increasing its concentration to a much higher value compared to its abundance in nature. The oxygen in nature has 3 stable isotopes: ^{16}O (99.759%); ^{17}O (0.037%) and ^{18}O (0.204%). The stable isotopes necessary for different applications are typically found in nature in very low concentrations in nature, and the necessity to increase their concentration occurs. The isotopic exchange reaction involves the reversible substitution of atoms between two different isotopic molecules. Its equation is expressed as (1):

$$AX + BX^* \leftrightarrow AX^* + BX \tag{1}$$

where X and X* are two isotopes of the same element which are interchanged between the AX and BX molecules (Axente et al, 1994). The separation via isotopic exchange, governed by the thermodynamic isotopic effect and characterized by the elementary separation factor (α), includes various reactions for ^{18}O isotope separation, notably the interaction between nitric oxides and aqueous solutions of HNO_3. In the case of using the system NO, NO_2-H_2O, HNO_3 as separation process, the NO, NO_2 circulate in counter-current with the HNO_3 solution, the isotopic exchange occurs according to the equation:

$$N^{16}O + H_2{}^{18}O \xleftrightarrow{HNO_3} N^{18}O + H_2{}^{16}O \tag{2}$$

The utilization of a separation plant (Sulaberidze et al., 2021), equipped with 2 separation columns, is being contemplated for the tangible implementation of the separation process involving the NO, NO_2-H_2O, HNO_3 system.

2. THE SEPARATION PLANT USED FOR ^{18}O ENRICHMENT

The ^{18}O isotope separation plant, used in the experimental procedures, is schematically presented in Fig. 1. The separation of ^{18}O is achieved through isotopic exchange within the NO, NO_2-H_2O, HNO_3. The separation cascade comprises two parts: the Primary Separation Column (PSC) and the Final Separation Column (FSC). The two columns have the same length (h = 1000 cm), but they have different diameters (PSC: d_1 = 50 mm, while the FSC: d_2 = 14 mm). PSC contains in its structure 4 equal sections (S11-S14) and FSC contains 5 equal sections (S21-S25). In order to highlight the positions in the two columns' heights, the (0r) axis is defined, presented in the schematic representations of the two columns from Fig. 1 lateral parts. In both cases, the (0r) axis has its origin at the center of the base transversal sections of the columns (PCBS in the PSC case and FCBS in the FSC case). Also, the (0r) axis has physical significance only inside the columns volume (bounded in the

upper part by their top sections: PCTS for PSC and FCTS for FSC).

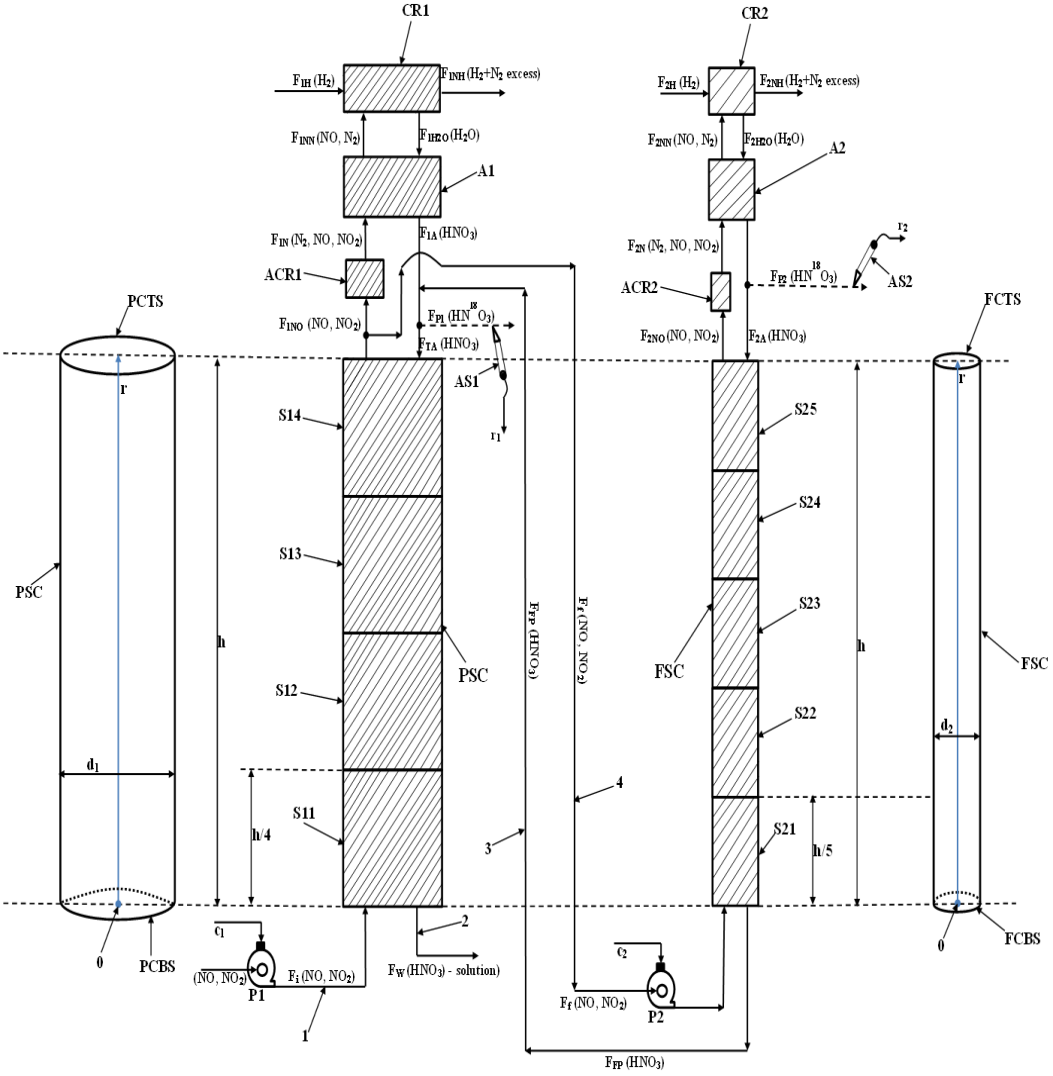

Fig. 1. The ^{18}O isotope separation plant.

Table 1. The separation plant step responses (in relation to time) experimentally obtained

Sample / Time and Response	1	2	3	4	5	6	7	8	9	10
Time [h]	0	150	233.92	309.653	375.742	451.785	531.617	619.117	702.941	727.573
PSC Response [%]	0.204	0.4549	0.4784	0.549	0.5804	0.6549	0.6902	0.7255	0.7725	0.7882
FSC Response [%]	0.204	0.7208	0.936	1.2462	1.408	1.728	2.0059	2.3294	2.608	2.8008

The supply of the separation cascade with NO and NO_2, obtained as waste from the ^{15}N isotope separation plant, is made at the PSC base through pipe 1 using the pump P1 (c_1 is the control signal which controls P1 operation). The waste, in the form of an HNO_3 solution, is removed from the base of the separation cascade via pipe 2 originating from the PSC. Using pipe 4 and the pump P2 (where c_2 is the control signal which controls P2 operation), the base of the FSC is supplied with NO and NO_2, which have a higher concentration of ^{18}O, acquired at the top of the PSC. The same quantity of ^{18}O isotope is returned from the FSC base to the PSC top, through pipe 3, under the form of HNO_3 solution. The two columns' interconnection through pipes 3 and 4 is essential for the operation of the two columns in a separation plant (without this interconnection, the two columns would operate independently). In both columns the NO, NO_2 and the HNO_3 circulate in counter-current and through the contact of the two chemical elements, the phenomenon of ^{18}O isotope enrichment occurs. In Fig. 1 are, also, highlighted the devices from the structure of the separation plant refluxing system.

The experimental data used in the modeling procedure are acquired during several experiments performed by using the

real separation plant (Mansourzadeh et al., 2024). The main difficulties in performing the experiments are: the extremely long duration of them (the main signals associated to the separation plant get steady after several months because of the high values of the time constants); the large number of the power plant parameters which have to be simultaneously monitored and controlled; the strong interdependency between the power plant parameters; the strong nonlinear behavior of the ^{18}O separation process; the risk of the failures which may arise during operation of any equipment from the power plant structure (if the failures are consistent then the risk of the experiment stop occurs and implicitly the risk of losing the entire ^{18}O production occurs, too) (Fisca et al., 2023) In Table 1, the separation plant step responses (in relation to time) experimentally obtained are presented. The two responses are referring to the evolutions of the concentration of ^{18}O at the tops of the PSC and FSC. Also, the values of the two step type signals applied at the inputs of the two separation columns are F_i = 880 l/h for PSC and F_f = 80 l/h in the case of FSC (the two input flows being nitric oxides flows – NO, NO_2). Table 1 reveals that the concentration of ^{18}O increases significantly faster with FSC compared to PSC, owing to FSC's ability to further separate the already isolated isotope. Also, from Table 1 it results that the experiment was halted after approximately 730 h by damage at one of the equipment from the structure of the PSC refluxing system. However, this aspect did not affect the validity of the acquired experimental data due to the fact that they are enough in order to be processed for determining the separation plant structure parameters. A crucial aspect that requires mentioning is that the performed experiments were made in the total reflux regime operation (in this operation regime, the product isn't retrieved from the separation plant, more exactly the F_{P1} and F_{P2} nitric acids flows (having an increased ^{18}O concentration) are equal to 0 ml/h). The ^{18}O concentrations presented in Table 1 are determined by using the AS1 and AS2 mass spectrometers.

3. MATHEMATICAL MODEL OF THE SEPARATION PLANT

The separation plant contains within its structure two sub-processes that are serially connected: the sub-process associated with PSC and the sub-process associated with FSC. The "black box" type representation of the separation cascade, highlighting the two sub-processes and the interdependencies between them, is presented in Fig. 2.

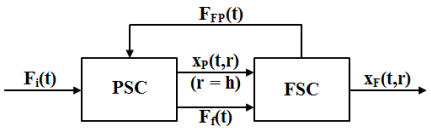

Fig. 2. The sub-processes.

The ^{18}O concentrations at the output of the two columns are notated with $x_P(t)$ and $x_F(t)$. The main input signal in PSC is considered the nitric oxides supplying flow $F_i(t)$ and the main output signal from PSC is considered $x_P(t)$. Also, the main input signals in FSC are considered $x_P(t)$ and the nitric oxides supplying flow $F_f(t)$, meanwhile the main output signal from FSC is considered $x_F(t)$. The $F_f(t)$ signal is modified due to the usage of P2 pump from Fig. 1 which is not figured in Fig. 2 due to its much faster dynamics. Also, the nitric acid flow F_{FP} which is circulated from FSC to PSC is proportional with $F_f(t)$ and it is figured in Fig. 2 in order to highlight the interdependency between the two columns operation. The processes associated both to PSC and FSC are distributed parameter nonlinear processes, a fact which implies the necessity of determining complex mathematical models which describe their operation. The property of distributed parameter processes results is due to the fact that the ^{18}O isotope concentrations in the two separation columns depend both on time (t) and on the "length" independent variable (r) ($x_P(t,r)$ and $x_F(t,r)$). The (r) is correlated to the (0r) Cartesian axes from Fig. 1 and highlights the positions in the two columns heights. Using r - the independent variable, the increasing evolution of the ^{18}O isotope concentration from the columns bases to their tops can be mathematically introduced in the plant model. The mathematical model is a hybrid one, more exactly its structure is analytically determined, but the model structure parameters are experimentally computed.

Below are the equations that outline the functioning of the separation plant. The dynamics of the two separation columns with respect to time (t) can be modeled by the following nonlinear differential equations:

- for PSC: $$T_1(F_i)\cdot\frac{d(x_{PI}(t))}{dt}+x_{PI}(t)=S_{PST}(F_i)\cdot x_0 \quad (3)$$

- for FSC: $$T_{2in}(F_f)\cdot\frac{d(x_{FI}(t))}{dt}+x_{FI}(t)=S_{FST}(F_f)\cdot x_{Pst} \quad (4)$$

where: the variables $x_{PI}(t)$ and $x_{FI}(t)$ denote the dynamic increases in ^{18}O concentrations at the tops of the two columns compared to the input concentrations (x_0 = 0.204% natural abundance of the ^{18}O, for PSC and $x_P(t)$ in the context of FSC). In (3), $T_1(F_i)$ is the time constant of PSC depending on the input signal F_i value. In the case of PSC, the model has the structure of a first order nonlinear system. The FSC operation can be, also, modeled as a first order nonlinear system using (4). $T_{2in}(F_f)$ is the intrinsic time constant of FSC depending on the input signal F_f value. If we singularize the time constants for certain values of F_i and F_f input signals, (3) and (4) can be solved, the resulting solutions being the output signals $x_{PI}(t)$ and $x_{FI}(t)$. Initially in (4), basing on the experimental results, the intrinsic time constant of FSC is introduced (the time constant of FSC in the case when FSC is operated independently by the separation cascade). In order to ensure the separation cascade model correctness, the adjustment of the $T_{2in}(F_f)$ value is necessary. Consequently, in the final form, in (4), the $T_2(F_f) = K_A \cdot T_{2in}(F_f)$ time constant is used instead of $T_{2in}(F_f)$, where K_A = 3.17 is the adjustment coefficient determined using an experimentally-iterative procedure. In (3) and (4), the functions $S_{PST}(F_i)$ and $S_{FST}(F_f)$ are given by: $S_{PST}(F_i) = S_P(F_i) - 1$ and $S_{FST}(F_f) = S_F(F_f) - 1$, where $S_P(F_i)$ and $S_F(F_f)$ represent the separations of PSC, respectively of FSC.

The two separations $S_P(F_i)$ and $S_F(F_f)$ are given by:

$$S_P(F_i(t)) = \alpha^{\frac{h}{HETP_P(F_i(t))}} \quad (5)$$

respectively

$$S_F(F_f(t)) = \alpha^{\frac{h}{HETP_F(F_f(t))}} \quad (6)$$

where $HETP_P(F_i(t))$ and $HETP_F(F_f(t))$ represent the Height of Equivalent Theoretical Plate functions associated to PSC and FSC. Also, the value $\alpha = 1.018$ represents the elementary separation factor of the ^{18}O. The exponents of (5) and (6) represent the Numbers of the Equivalent Theoretical Plates of the 2 separation columns (PSC and FSC). The $HETP_P(F_i(t))$ and $HETP_F(F_f(t))$ are given by (7) and (8).

$$\begin{cases} HETP_P\big(F_i(t)\big) = HETP_{PC} + K_{P1} \cdot (F_i(t) - F_{iC}), \\ \qquad for\ F_i(t) \le F_{iC} \\ HETP_P\big(F_i(t)\big) = HETP_{PC} + K_{P2} \cdot (F_i(t) - F_{iC}), \\ \qquad for\ F_i(t) > F_{iC} \end{cases} \tag{7}$$

$$\begin{cases} HETP_F\left(F_f(t)\right) = HETP_{FC} + K_{F1} \cdot \big(F_f(t) - F_{fC}\big), \\ \qquad for\ F_f(t) \le F_{fC} \\ HETP_F\left(F_f(t)\right) = HETP_{FC} + K_{F2} \cdot \big(F_f(t) - F_{fC}\big), \\ \qquad for\ F_f(t) > F_{fC} \end{cases} \tag{8}$$

In (7) and (8), the constant values $HETP_{PC}$ and $HETP_{FC}$ are minimal (critical) values of the $HETP_P(F_i(t))$ and $HETP_F(F_f(t))$ functions obtained for the critical values F_{iC} and F_{fC} of the two input nitric oxides flows. Also, K_{P1}, K_{P2}, K_{F1} and K_{F2} are proportionality constants experimentally determined. In (4), the x_{Pst} signal represents the steady state value of the ^{18}O concentration at the top of PSC, for a certain value of the nitric oxides input flow F_i and is given by:

$$x_{Pst}(F_i) = x_0 \cdot \alpha^{\frac{h}{HETP_P(F_i)}} \tag{9}$$

To highlight the variation in ^{18}O concentration with respect to heights (along the 0r axes) of the the PSC and FSC, the 2 separation columns "height constants" are defined in (10) and (11).

$$\begin{cases} R_1\big(F_i(t)\big) = R_{PC} + K_{PR1} \cdot (F_i(t) - F_{iC}), \\ \qquad for\ F_i(t) \le F_{iC} \\ R_1\big(F_i(t)\big) = R_{PC} + K_{PR2} \cdot (F_i(t) - F_{iC}), \\ \qquad for\ F_i(t) > F_{iC} \end{cases} \tag{10}$$

$$\begin{cases} R_2\left(F_f(t)\right) = R_{FC} + K_{FR1} \cdot \big(F_f(t) - F_{fC}\big), \\ \qquad for\ F_f(t) \le F_{fC} \\ R_2\left(F_f(t)\right) = R_{FC} + K_{FR2} \cdot \big(F_f(t) - F_{fC}\big), \\ \qquad for\ F_f(t) > F_{fC} \end{cases} \tag{11}$$

In (10) and (11), $R_1(F_i(t))$ and $R_2(F_f(t))$ are the "height constants" of PSC, respectively of FSC, R_{PC} and R_{FC} are their critical values (obtained for the critical values F_{iC} and F_{fC} of the two input nitric oxides flows). Also, K_{PR1}, K_{PR2}, K_{FR1} and K_{FR2} are proportionality constants. It can be remark that the functions presented in (7), (8), (10) and (11) exhibit linearity across their domains or values, but display nonlinearity across their entire domains of definition. Consequently, the final form of the ^{18}O isotope concentrations, in the two columns from the separation plant structure, depending on both (t) and (r) independent variables, are given by (12) and (13):

$$x_P(t,r) = x_{PI}(t) \cdot \frac{F_{RP}(r) - 1}{F_{RP}(r = h) - 1} + x_0 \tag{12}$$

$$x_F(t,r) = x_{FI}(t) \cdot \frac{F_{RF}(r) - 1}{F_{RF}(r = h) - 1} + x_P(t, r = h) \tag{13}$$

where the $F_{RP}(r)$ and $F_{RF}(r)$ functions forms are presented in (14) and (15):

$$F_{RP}(t, F_i(t)) = e^{\frac{r}{R_1(F_i(t))}} \tag{14}$$

$$F_{RF}\big(t, F_f(t)\big) = e^{\frac{r}{R_2(F_f(t))}} \tag{15}$$

Also, the notations from (16) and (17) can be made:

$$F_{rPSC}(r) = \frac{F_{RP}(r) - 1}{F_{RP}(r = h) - 1} \tag{16}$$

$$F_{rFSC}(r) = \frac{F_{RF}(r) - 1}{F_{RF}(r = h) - 1} \tag{17}$$

All parameters of the power plant appearing in the equations presented earlier are determined experimentally. The $T_1(F_i)$ and $T_2(F_f)$ time constants dynamics are determined based on experimental data of the type of those presented in Table 1, obviously after applying their filtering, after approximating the most probable curves that average them with high accuracy and after repeating the identification procedure for the data resulted from several experiments. In the case of both time constants, a decreasing monotonously nonlinear variation, at the input nitric oxides flows increasing, resulted. The K_{P1}, K_{P2}, K_{F1} and K_{F2} proportionality constants are identified based on the steady state values of the PSC and FSC concentrations, obtained for different constant input nitric oxides flows. Using the mentioned steady state values, based on an inverse mathematical processing of equations (5) and (6) (knowing that the obtained concentrations are given by the mathematical products between the initial concentrations values and the corresponding separations), the HETP functions values resulted for the input nitric oxides flows that were applied. Consequently, by analyzing and processing the obtained HETP functions values, their dependency by the corresponding input flows were determined and the K_{P1}, K_{P2}, K_{F1} and K_{F2} proportionality constants resulted. Using these coefficients, the possibility of the complete direct definition of the two separations from (5) and (6) occurs. The evolutions of the two separation functions in relation to the associated input nitric oxides are nonlinear ones on the entire definition domain. Also, these evolutions have a monotony change in the points F_{iC} and F_{fC}. On the resulting subdomains, the mentioned evolutions are nonlinear, too, but they do not present monotony change on the two subdomains. The K_{PR1}, K_{PR2}, K_{FR1} and K_{FR2} proportionality constants are identified based on the exponential increasing distribution of the ^{18}O from the two separation columns lower parts to their tops, based on the ^{18}O isotope experimentally determined concentrations (measured at the two separations columns tops).

To simulate the mathematical model proposed earlier, the instantaneous values of the $S_{PST}(F_i)$, $T_1(F_i)$, $R_1(F_i)$, respectively of $S_{FST}(F_f)$, $T_2(F_f)$ and $R_2(F_f)$ have to be available. In this context, artificial intelligence techniques relying on neural networks are employed to understand the dynamics of the specified functions.

The main advantages of using neural networks (neural models) are: their higher generated accuracy than other types of models (for example polynomial models or Spline models; the accuracy generated by the neural networks becomes much higher near the points in which a part from the mentioned functions present monotony changes); the fact that they represent a compact model for approximating more than one function in the same time; in their training procedure, a large number of data can be processed. To understand the dynamics of the parameters associated to PSC operation, respectively to FSC operation, two neural networks are used, having the general representation from Fig. 3.

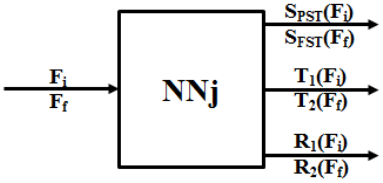

Fig. 3. The representation of the two neural networks.

In Fig 3, "j" can represent either PSC or FSC. When j = PSC, the signals above the arrows are applicable, and when j = FSC, the signals below the arrows are applicable. NNj is defined as a feed-forward fully connected neural network (Muresan et al., 2018; Sita et al., 2018; Muresan et al., 2015; Osuolale et al., 2016) comprising: a hidden layer with 24 nonlinear neurons (utilizing a bipolar sigmoid activation function) and an output layer with 3 neurons (employing a linear activation function). The training of NNPSC and NNFSC is made using 1550 pairs of input-output data samples. The set target Mean Square Errors (MSE; the considered quality indicator), for all neural networks output signals, was 10^{-5} which is a consistently lower value than the necessary ones for obtaining a high accuracy of the proposed model (in the cases of $S_{PST}(F_i)$ and $S_{FST}(F_f)$ MSE values proportionally with 10^{-4} are considered enough accurate. In the cases of $R_1(F_i)$ and $R_2(F_f)$ values proportionally with 10^{-2} are considered enough accurate. For $T_1(F_i)$ and $T_2(F_f)$ values proportionally with 10^{-5} are considered enough accurate due to the fact that these parameters do not have monotony change). The total number of epochs was set to 30000 and, for training, the Levenberg-Marquardt algorithm was used. The achieved performances are presented in Table 2.

Table 2. The performances generated by the two neural networks.

Neural Network	NNPSC			NNFSC		
Output from NN	$S_{PST}(F_i)$	$T_1(F_i)$	$R_1(F_i)$	$S_{FST}(F_f)$	$T_2(F_f)$	$R_2(F_f)$
Obtained MSE	$8.97 \cdot 10^{-4}$	$9.15 \cdot 10^{-5}$ h	$0.91 \cdot 10^{-2}$ cm	$7.83 \cdot 10^{-4}$	$7.48 \cdot 10^{-5}$ h	$3.59 \cdot 10^{-2}$ cm

The 2 pre-trained neural solutions produce the subsequent output signals, expressed in a generalized form:

$$N_j = HLW_j \cdot \left[bs\left(ILW_j \cdot F_k(t) + HLB_j\right)\right] + OLB_j \qquad (18)$$

where, in this case too, $j \in \{PSC; FSC\}$, $k \in \{i; f\}$ (in the case of PSC, the input nitric oxides flow is $F_i(t)$ and in the case of FSC, it is $F_f(t)$) and "bs" represents the bipolar sigmoid activation function (the hyperbolic tangent activation function.

The output vectors are $N_j(3\times1) = [S_j(F_i)\ T_V(F_i)\ R_V(F_i)]^\tau$, where V = 1 if j = PSC and V = 2 if j = FSC and "τ" represents the notation which signifies the application of the transpose operation. The $ILW_j(24\times1)$ vectors contain the two neural networks input layer weights solutions, the $HLB(3\times24)$ matrices contain the two neural networks hidden layer weights solutions, the $HLB_j(24\times1)$ vectors contain the two neural networks hidden layer biases solutions, respectively $OLB_j(3\times1)$ vectors contain the two neural networks output layer biases solutions (the term "solution" is referring in all cases to the training solutions). Consequently, the implementation of the equations associated to the proposed mathematical model is presented in Fig. 4.

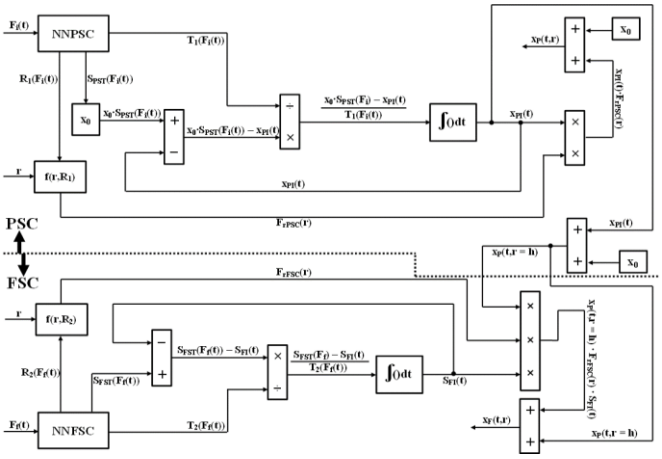

Fig. 4. The implementation of the equations associated to the model of the separation plant.

4. THE SIMULATIONS RESULTS

The simulations results presented in this section are made in MATLAB/Simulink. In Fig. 5, five open loop step responses of the separation plant are comparatively presented. The pairs of input flows in the columns are relevant in highlighting the separation efficiency. Practically, the responses from Fig. 5 represent the evolutions in relation to time of the ^{18}O isotope concentration at the FSC output.

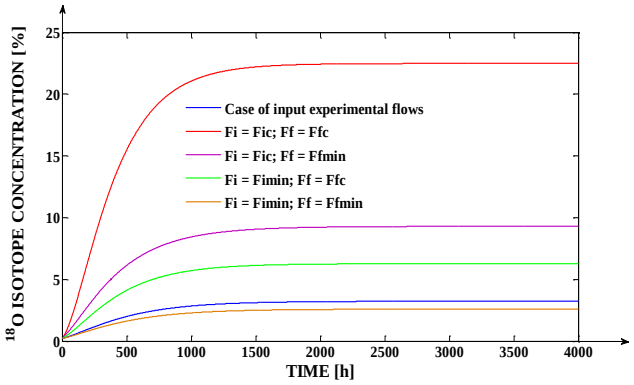

Fig. 5. Comparing five open-loop step responses of the plant.

The equilibrium values (Unguresan and Niac, 2011) of the responses from Fig. 5 are consolidated in Table 3.

Table 3. The steady state values of the responses from Fig. 5.

The input flows in the PSC and FSC	F_{ic}, F_{fc}	F_{ic}, F_{fmin}	F_{imin}, F_{fc}	F_{imin}, F_{fmin}	F_i = 880 l/h, F_f = 80 l/h
The steady state values of the $x_F(t, r = h)$ signal	22.4771 %	9.2903 %	6.272 %	2.5924 %	3.2311 %

The maximum concentration (22.4771 %) is obtained for the pair of critical flows F_{ic} and F_{fc} which generate the maximum separation, respectively the minimum concentration (2.5924 %) is obtained for the pair of minimum flows F_{imin} and F_{fmin}. Also, in Fig. 5 are presented other three cascade responses in the case of using different combinations of intermediary flows values (including the values used in the experiments which generated the curves used in the identification procedure: F_i = 880 l/h and F_f = 80 l/h). Consequently, the proposed model can be used to simulate the separation process for any possible values of the two input signals. By using the appropriate values for the two input flows, any concentration value enclosed in the domain [2.5924; 22.4771] % can be obtained.

In this context, through iterative simulations of the proposed model, the two input flows which generate an imposed ^{18}O isotope concentration at the FSC output can be determined. This aspect represents an important technological advantage since, by using the proposed model, the operators have access to the cascade operation parameters necessary to be used in order to obtain an imposed ^{18}O isotope concentration. Another advantage is the fact that by obtaining the imposed ^{18}O isotope concentration, the later thinning procedures can be avoided. In Fig. 5, the fact that the five curves have different settling times results, too. For a better highlighting of this phenomenon, the comparative graph from Fig. 6 is presented.

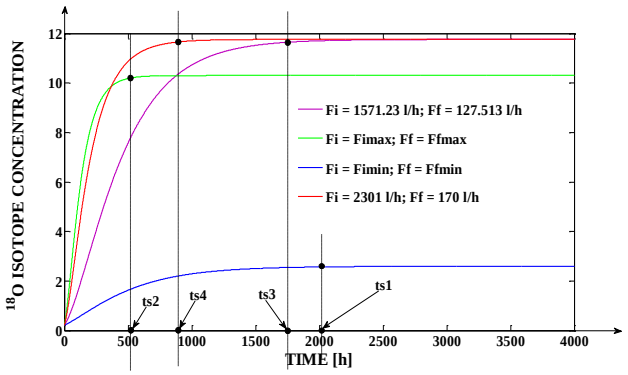

Fig. 6. The settling time variation.

Fig. 6 contains four responses of the plant: the slowest one (for $F_i = F_{imin}$ and $F_f = F_{fmin}$, resulting t_{s1}), the fastest one (for $F_i = F_{imax}$ and $F_f = F_{fmax}$, resulting t_{s2}) and two intermediary responses (referring to the process speed) which generate the same steady state value $x_F(t, r = h)$ = 11.762 % of the ^{18}O isotope concentration (for F_i = 1571.23 l/h and F_f = 127.513 l/h, respectively for F_i = 2301 l/h and F_f = 170 l/h).

The settling times of the obtained responses are listed in Table 4. Additionally, Table 4 includes the value of the settling time (t_{s5}) obtained for the critical input flows (F_{ic} and F_{fc}).

Table 4. The Centralizer with the settling times of the responses presented in Fig. 6.

The input flows in the PSC and FSC	F_{imin}, F_{fmin}	F_{imax}, F_{fmax}	F_i = 1571.23 l/h, F_f = 127.513 l/h	F_i = 2301 l/h, F_f = 170 l/h	F_{ic}, F_{fc}
Separation cascade settling time	t_{s1} = 2018.8 h	t_{s2} = 516.36 h	t_{s3} = 1745.33 h	t_{s4} = 867.71 h	t_{s5} = 1564.43 h

The fact that $t_{s2} << t_{s1}$ is due to the consistent decrease of both $T_2(F_f)$ and $T_1(F_i)$ time constants for high values of the two flows. Consequently, the minimum settling time t_{s2} is obtained for the maximum flows. In order to avoid the flooding regime (which is a hard constraint), it must be avoided the increase the two flows over the maximum values (more exactly a lower value for the settling time cannot be obtained). The slowest response having the settling time t_{s2} is obtained for the minimum flows, for which the functions $T_2(F_f)$ and $T_1(F_i)$ have the maximum values. In order to avoid the insufficient damping of the columns steel packing (which is, also, a hard constrain), it must be avoided the decrease the two flows under the minimum values (more exactly a higher value for the settling time cannot be obtained). The two simulations which generate the same $x_F(t, r = h)$ = 11.762 % output concentration are made in order to prove that it is possible to obtain the same product much efficiently considering the settling time as the essential performance. Practically, with the cost of higher input flows, we can obtain at the separation cascade output the same ^{18}O isotope concentration in a much shorter period (in the given example, $t_{s4} << t_{s3}$ with 877.62 h, an advantage which offers the possibility of producing the same quantity of product in a much shorter period). This separation cascade property is an essential premise for the design of a control system for the ^{18}O isotope concentration. In the case of applying the critical flows as input signals, we obtain the t_{s5} settling time (Fig. 5) which is an intermediary value between t_{s2} and t_{s1}. On the other side, using F_{ic} and F_{fc}, the highest value of the product concentration is obtained (Fig. 5 and Table 3). The intricacy of the process and implicitly the complexity of the future designed concentration control system results from the high number of the available degrees of freedom implied by the input flows variations (separation, time constants, length constants) and from the nonlinear interdependencies between them.

Another important phenomenon which occurs in the plant operation is the variation of ^{18}O concentration, with respect to the positions in the 2 columns heights. In this context the comparative graph from Fig. 7 is presented, containing 10 responses of 2 columns from structure of the separation plant. In the lower part of Fig. 7, the significance of the used color code is highlighted. Additionally, the steady-state values of the responses depicted in Fig. 7 are consolidated in Table 5. The simulations results, presented in Fig. 6 and in Table 5, are made considering the NO and NO_2 input flows in the 2 columns: F_i = 1000 l/h and F_f = 160 l/h.

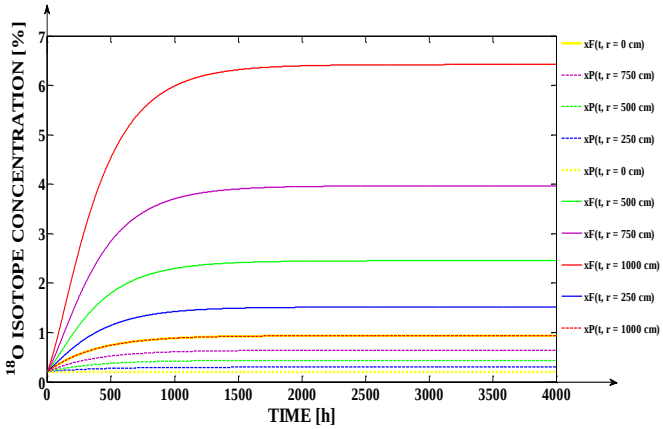

Fig. 7. The ^{18}O isotope concentration with respect to the positions in the PSC and FSC columns heights.

Table 5. The steady state values of the responses from Fig. 7.

	The input flows in the PSC and FSC: F_i = 1000 l/h and F_f = 160 l/h	
r independent variable value	The steady state values of the $x_P(t, r)$ signal	The steady state values of the $x_F(t, r)$ signal
r = 0 cm	0.204 %	0.9364 %
r = 250 cm (r = h/4)	0.2986 %	1.5152 %
r = 500 cm (r = h/2)	0.4371 %	2.4518 %
r = 750 cm (r = 3·h/4)	0.6397 %	3.9677 %
r = 1000 cm (r = h)	0.9364 %	6.4211 %

Analyzing the results from Fig. 7 and Table 5, the increasing evolution of the ^{18}O isotope concentration from the base to the top of the two columns can be remarked. The exponential evolution of the output signals from the two separation columns (highlighted in (12) and in (13) due to the $F_{rPSC}(r)$ and $F_{rFSC}(r)$ functions) is proven in Fig. 8. In Fig. 8, the $x_P(t = t_f, r)$ and $x_F(t = t_f, r)$ signals variation is presented (in relation to the independent variable (r)).

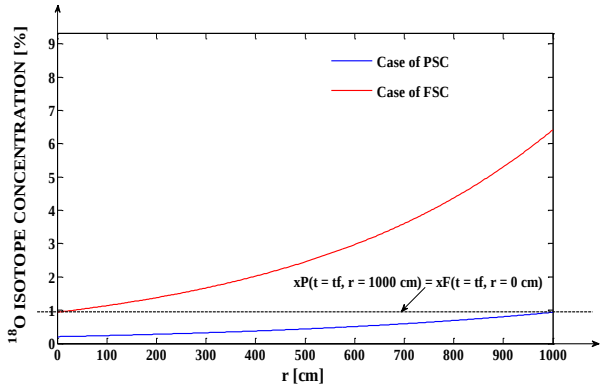

Fig. 8. The ^{18}O isotope concentration evolution in the two separation columns, in relation to the independent variable (r).

The two curves from Fig. 8 are obtained using the data centralized in Table 5 (obviously for the same F_i = 1000 l/h and F_f = 160 l/h input flows). In Fig. 8 is, also, highlighted the fact that the concentration of the ^{18}O isotope at the PSC output is equal to the concentration of the ^{18}O isotope at the FSC input ($x_P(t = t_f, r = h) = x_F(t = t_f, r = 0)$). In Fig. 8 this aspect is shown through the usage of the dashed line which corresponds to the concentration value of 0.9364 % (the last value from the second column of Table 5 and the first value from the third column of Table 5). As it results from Fig. 8, the blue curve (associated to the x_P signal evolution) intersects the dashed line for r = 1000 cm and the red curve (associated to the x_F signal evolution) intersects the dashed line for r = 0 cm. From the physical perspective, the equality between $x_P(t = t_f, r = h)$ and $x_F(t = t_f, r = 0)$ signals is because FSC is supplied with the product obtained from PSC.

To demonstrate the need for a future ^{18}O isotope concentration control system, we simulate the impact of an external disturbance during separation plant operation (Golnaraghi et al., 2009; Love, 2007; Iraola et al., 2021). The simulation is made using the same F_i = 1000 l/h and F_f = 160 l/h inlet flows as depicted in Figs. 7 and 8, respectively as in the case of Table 5. The exogenous disturbance affects (technically) the pump P1 (from Fig. 1) operation after the moment t_d = 3000 h, implying a fast decrease of the F_i signal from the initial value of 1000 l/h to the value of 900 l/h (an equivalent decrease of F_i with 100 l/h). Considering these remarks, the separation plant response is presented in Fig. 9. From Fig. 9 results directly the fact that the disturbance effect is not rejected. The disturbance effect consists in the separation plant response's progressive decrease after the moment t_d, to the new steady state value (5.9425 %). Practically, the disturbance effect is the decrease of the $x_F(t)$ signal with almost 0.5 %, a significant value which implies a major technological disadvantage (the ^{18}O isotope concentration cannot be maintained at the imposed value at which the isotope can be commercialized). In this context, the design of an automatic system for the ^{18}O isotope concentration is proven, thus becoming a necessity.

The simulation from Fig. 9 represents only one example of disturbance which can occur in the functioning of the plant, but in the real power plant case other types of disturbances can occur, too. An efficient control system would have two important objectives: firstly, to maintain the ^{18}O isotope concentration at the set point value and secondly to mitigate the impacts of all disturbances that arise during the operation of the separation cascade.

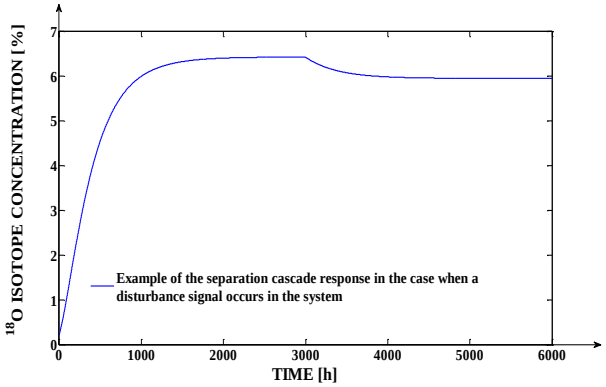

Fig. 9. The response when the disturbance occurs in the system.

Considering the input signals F_i = 1807.4 l/h and F_f = 141.9 l/h, the comparative graph between the most probable response of the separation cascade and the responses of the separation cascade models using the Neural Networks, respectively using the Spline approximations (simultaneously, for both $S_{PST}(F_i)$ and $S_{FST}(F_f)$ functions), is presented in Fig. 10.

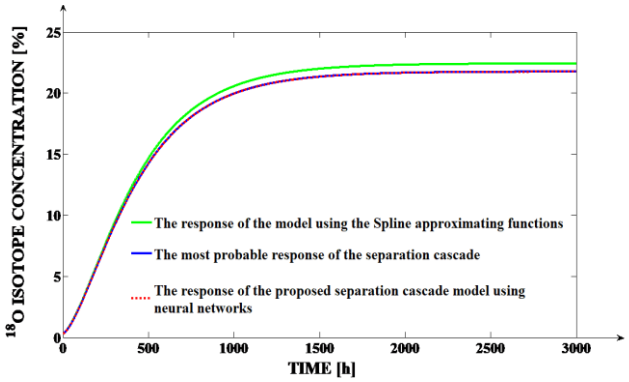

Fig. 10. The advantage of using neural networks in comparison with Spline approximations.

The much higher accuracy generated by the usage of the proposed neural networks in the model structure is evident by the precise superposition of the responses highlighted with the blue and red colors (in Fig. 10). This aspect is, also, proven through the analysis of the MSE values. Consequently, using 3001 pairs of values of the responses from Fig. 10, the MSE value between the blue and the red curves is $3.5 \cdot 10^{-3}$ % which is much lower than the MSE value between the blue and the green curves ($6.3 \cdot 10^{-1}$ %).

5. CONCLUSIONS

The proposed mathematical model is accurately validated by comparing its simulation results with experimental data. It fully captures the dynamics of ^{18}O isotope concentration within the separation cascade as a nonlinear distributed parameter model. Linearization techniques, commonly used in literature, were intentionally avoided to maintain model precision. Employing neural networks to understand the dynamics of separation cascade structural parameters, especially concerning input flows in the 2 separation columns, significantly improves the accuracy of the model. Neural networks offer greater accuracy in comparison to alternative modeling techniques. The proposed model offers several significant technological advantages, including:

- the ability to ascertain the suitable values of input flows in the two columns to achieve a specific desired level of ^{18}O concentration at the output of the separation cascade;

- the possibility of designing and implementing an automatic control system for the concentration of ^{18}O capable of achieving high control performances;

- the possibility to control the ^{18}O isotope concentration in certain positions in the two separation columns height, which implies the possibility to extract the product from intermediary extraction points, in relation with the two separation columns heights; this aspect is important in the situations when the product concentration has to be rapidly changed due to an urgent demand from a client and the delivering term is shorter than the separation cascade settling time to a new steady state regime;

- the possibility to include the model as separation cascade reference model in a more advanced control structure (the structure based on IMC (Internal Model Control Strategy) or in fault tolerant control structures;

- the possibility to extend the control systems with the functionality of reducing the separation cascade energy consumption;

- the ability to simulate the impacts of disturbances that occur within the system.

The methods employed for identifying the parameters of the proposed model structure are explicitly outlined in Muresan et al., 2024.

REFERENCES

Abrudean, M., Axente, D. and Baldea, A. (1981). Enrichment of ^{15}N and ^{18}O by Chemical Exchange Reaction Between Nitrogen oxide (NO, NO_2) and Aqueous Nitric Acid, *Isotopenpraxis*, 17 (11), pp. 377- 382.

Abrudean, M., Axente, D., Bâldea, A. and Jalobeanu, M. (1978). A Model of Calculation for flow-rate and Concentration for ^{18}O Separation Plant by NO, NO_2-H_2O, HNO_3 Isotopic exchange, *Revista de Chimie*, 29(10), pp. 953-955.

Axente, D., Abrudean, M. and Bâldea, A. (1994). *^{15}N, ^{18}O, ^{10}B, ^{13}C Isotopes Separation Trough Isotopic Exchange*, Sci. Book House, Cluj-Napoca, Romania, pp. 122-238.

Cohen, K. (1951). *The Theory of isotope Separation as Applied to the Large Scale Production of ^{235}U*, New York.

Dulf, E, Unguresan, M. L., Gligan, M., Festila, C. (2006). Operational models of the cryogenic distillation column for (^{13}C) isotope, *IEEE-TTTC International Conference on Automation, Quality and Testing, Robotics*, pp.159-162.

Fişcă, M., Abrudean, M., Muresan, V., Unguresan, M.L., Clitan, I., Cordos, R., Stancioi, C. (2023). Modeling and Control of the ^{18}O Isotope Separation Plant, *Journal of Control Engineering and Applied Informatics*, 25 (1), pp. 101-112.

Golnaraghi, F. and Kuo, B. C. (2009). *Automatic Control Systems*, 9th ed. John Wiley and Sons Ltd. Chichester, United Kingdom.

Iraola, E., Nougués, J. M., Sedano, L., Feliu, J. A. and Batet, L. (2021). Dynamic Simulation Tools for Isotopic Separation System Modeling and Design, *Fusion Engineering and Design*, 169, 112452.

Love, J. (2007). *Process automation handbook: A Guide to Theory and Practice*. Springer, United Kingdom.

Mansourzadeh, F., Shadman, M. M., Ghazanfari, V. (2024), Advancements in numerical modeling of ideal multicomponent isotope separation Cascades: A comparative study, *Nuclear Engineering and Design*, 424, 113248.

Muresan, M., Abrudean, M. and Moga, D. (2015). Modeling, Simulation and Control of a Nonlinear Distributed Parameter Isotope Separation Process, *9th IFAC*

Symposium on Control of Power and Energy Systems (CPES 2015), New Delhi, India, 48(30), pp. 191-196.

Muresan, V., Abrudean, M., Unguresan, M. L. and Coloşi, T. (2018). Control of the Isotopic Exchange for ^{18}O Isotope Production, *IEEE 12th International Symposium on Applied Computational Intelligence and Informatics* (SACI 2018), 17-19 May 2018, Timişoara, România.

Muresan, V., Chifor, L., Abrudean, M., Unguresan, M. L., Clitan, I. and Sita, V.I. (2024). Identification of the Structures Parameters of an ^{18}O Separation Cascade, using Combined Classical Methods and Neural Networks, Submitted to *International Conference on Control & Automation* (ICCA).

Osuolale, F. N. and Zhang, J. (2016). Energy efficiency optimisation for distillation column using artificial neural network models. *Energy*, 106, pp. 562-578.

Sita, V., Mureşan, V., Abrudean, M., Unguresan, M.-L.and Clitan, I. (2018). ^{18}O Isotope Concentration Control, 15th *International Conference on Informatics in Control, Automation and Robotics (ICINCO)*, Porto, Portugal.

Sulaberidze, G. A., Smirnov, A. Y., Borisevich, V. D., Zeng, S., Jiang, D. (2021). Classification of model cascades for separation of multicomponent isotope mixtures, *Separation Science and Technology*, 56(6), 1060–1070.

Unguresan, M. L., Niac, G. (2011). Pre-equilibrium Kinetics. Modeling and Simulation, *Russian Journal of Physical Chemistry*, 85 (4), pp. 549-556.